

Article

# Sensitivity of Offshore Tropical Cyclone Wave Simulations to Spatial Resolution in Wave Models

Xuanyu Chen \*, Isaac Ginis and Tetsu HaraGraduate School of Oceanography, University of Rhode Island, Narragansett, RI 02882, USA;  
iginis@uri.edu (I.G.); tetsuhara@uri.edu (T.H.)

\* Correspondence: xychen@my.uri.edu

Received: 27 August 2018; Accepted: 30 September 2018; Published: 11 October 2018



**Abstract:** This study investigated and quantified the sensitivity of tropical cyclone (TC) wave simulations in the open ocean to different spatial resolutions ( $1/3^\circ$ ,  $1/6^\circ$ ,  $1/12^\circ$  and  $1/24^\circ$ ) using two wave models, WAVEWATCH III (WW3) and Simulating WAVes Nearshore (SWAN). Six idealized TCs of different radii of maximum winds (25 km and 50 km), and of different translation speeds (3 m/s, 6 m/s and 9 m/s) were prescribed to force these two wave models. Results from both models show that the coarsest resolution ( $1/3^\circ$ ) introduces significant errors in both the significant wave height (SWH) and the mean wavelength. Moreover, results reveal that sensitivity to spatial resolution strongly depends on storm characteristics. Waves simulated under the small (25 km) and fast moving (9 m/s) TC show the largest sensitivity to the coarse spatial resolutions. With the  $1/3^\circ$  resolution, maximum SWH can be underestimated by as much as 6% in WW3 and 16% in SWAN compared to those with the  $1/24^\circ$  resolution. These findings from the idealized TC simulations are further confirmed by wave simulations under a historical storm. Our analysis also demonstrates that spatial smoothing of the input wind field with coarse grids is not the only reason for the errors in wave simulations.

**Keywords:** sensitivity; spatial resolution; extreme hurricane waves; storm surge-wave coupling

## 1. Introduction

Surface gravity waves under extreme conditions such as tropical cyclones (TCs) have been of practical and scientific interest for over a half century, since the pioneering paper by Barber and Ursell [1]. For engineers and weather forecasters, it is essential to accurately predict the height of extreme waves for safety of seafaring navigation, design and protection of marine structures and public safety. For scientists, these extreme TC waves are important because they may impact the coupled ocean–atmosphere system by modifying the air–sea fluxes and near surface turbulent processes.

Recent studies have shown that including surface wave effects in storm surge modeling is important because waves exchange momentum with ocean currents via the radiation stress ([2–5]). For example, a coupled storm surge-wave model system was developed by Dietrich et al. [3], in which the radiation stress is computed by the SWAN model and is passed to the ADvanced CIRCulation (ADCIRC) model. In addition, recent studies suggest that wind stress (or drag coefficient), which forces the storm surge model, may be strongly dependent on sea-states, and that accurate estimation of wind stress requires incorporating wave spectra from third generation wave models [6,7].

In the state-of-the-art coupled storm surge-wave models (ADCIRC-SWAN [3,8,9] and FVCOM-SWAVE [4]), both wave and storm surge simulations are performed on a common unstructured grid, where the spatial resolution is high in the nearshore region but it rapidly decreases toward the open ocean for computation efficiency. For example, in the ADCIRC-SWAN operational storm surge modeling system [10,11], simulations are conducted using a resolution coarser than 33 km

in the open ocean (Figure 1). While such a resolution is likely sufficient for storm surge prediction, it is unclear whether it is sufficient for accurate wave simulations under complex TC wind fields.

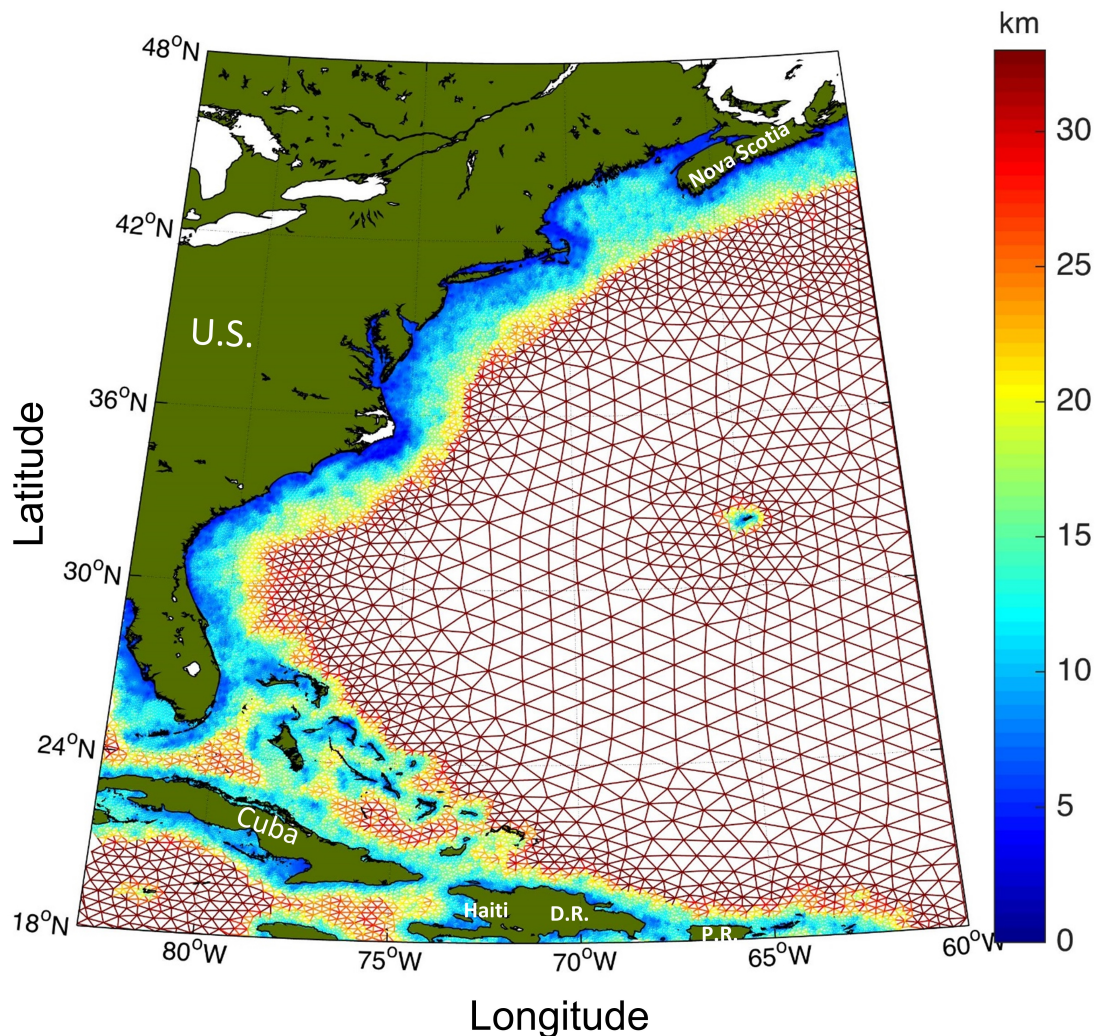


**Figure 1.** Spatial resolution of an unstructured grid in western North Atlantic region used in ADCIRC Surge Guidance System (ASGS).

There have been few studies directly addressing the wave model performance with different spatial resolutions. Kerr et al. [12] investigated the coupled ADCIRC-SWAN model sensitivity to the mesh resolution, topographical details and other factors during Hurricane Ike (2008). By comparing the SWAN wave simulations generated with two meshes of different resolutions against observational data, they concluded that, in the open Gulf, a moderate resolution (10–30 km) wave model can produce accurate wave characteristics. However, this conclusion was based on only one case study of a relatively large-size hurricane.

Xu et al. [13] modeled tropical cyclone waves under three typhoons in South China Sea using WW3 and compared simulated wave characteristics to buoy observations. They discussed sensitivity to spatial resolution in a three nested-mesh configuration ( $1/4^\circ$ ,  $1/8^\circ$  and  $1/12^\circ$ ) and reported that the grid resolution was not critical if the resolution of wind forcing remained coarse. However, they did not perform quantitative evaluation of the model sensitivity to spatial resolution.

Currently, wave simulations in open ocean are carried out with a wide range of spatial resolutions for different applications. The European Centre for Medium-Range Weather Forecasts (ECMWF) operates the High RESolution Wave Model (HRES-WAM) on a  $1/8^\circ$  resolution grid (Haiden et al. [14]).

The NOAA Hurricane Wave Model uses a  $1/10^\circ$  resolution (personal communication with Dr. Jessica Meixner). However, some operational and research wave models use coarser resolutions. For example, the NOAA operational global wave forecasts using the WW3 model, are carried out with  $1/2^\circ$ – $1/6^\circ$  resolutions in most regions (Figure 1 in Chawla et al. [15]). In a recent global climate study of TC-generated extreme waves based on CMIP5 multi-model ensemble (Shimura et al. [16]), the WW3 model is used with a resolution of 60 km. Tolman and Alves [17] developed a continuously moving grid version of the WW3 model to resolve TC wave conditions at high spatial resolution. This version of WW3 is designed only for offshore TC waves and has not been widely used in academic research and practical applications.

There is no doubt that higher spatial resolution produces more accurate TC wave simulations. However, for computational efficiency, TC wave modeling is still often performed on relatively coarse grid systems. To choose an optimal spatial resolution based on an acceptable error threshold for a given application, it is desirable to conduct a thorough quantitative evaluation of the wave model errors associated with various spatial resolutions in offshore TC wave simulations. Such information is valuable not only for coupled storm surge-wave modeling but also for other applications, such as global weather and climate models coupled with surface wave models.

In this study, we quantified for the first time the sensitivity of offshore TC wave simulations to spatial resolution by conducting systematic experiments under six idealized TCs with different characteristics, including storm size and translation speed. All experiments were performed separately with two widely used wave models, WW3 and SWAN. To complement the idealized experiments, a historical hurricane case was used to examine the effect of spatial resolution on wave simulations.

In this study, we did not attempt to validate the TC wave simulations against observations. This is because wave model results under TCs strongly depend on the parameterizations of the forcing terms (the wind forcing and the whitecap dissipation, in particular) in the wave models, as demonstrated by Liu et al. [18]. Here, we focus on investigating model sensitivity to different spatial resolutions, with one fixed (standard) setting of forcing parameterizations in each wave model.

## 2. Methods

### 2.1. Wave Models

Two widely used third-generation wave models, WAVEWATCH III (version 5.16) [19] and SWAN (version 41.01) [20], were utilized for this study. Both models solve the wave action equations, but WW3 solves for a directional wavenumber spectrum with an explicit numerical scheme, while SWAN solves for a directional frequency spectrum with an implicit numerical scheme [19,20]. Originally, WW3 was developed for simulating waves in the open ocean, while SWAN was optimized for simulating waves in coastal waters with more advanced shallow water physics. However, shallow water physics similar to that in SWAN has been introduced into WW3 since its version 4.18.

In both models, frequency is discretized into 40 bins, ranging from 0.0285 to 1.1726 Hz with a logarithmic increment factor of 1.1, while direction is discretized into 24 equally-spaced bins, following Fan et al. [21] and Reichl et al. [7]. In WW3, the wind input term together with the whitecapping dissipation term developed by Ardhuin et al. [22] (referred to as ST4 hereafter) is used. In ST4, the steepness-induced wave breaking (whitecapping) parameterization is saturation-based and includes the effect of cumulative breaking, independent of any prescribed spectral shape. The wind input parameterization in ST4 takes the positive part of parameterization in Janssen [23]. The wind input at high frequency and high winds is reduced, resulting in reduction of the drag coefficient at high winds. [19] The nonlinear interaction term is computed with the standard discrete interaction approximation (DIA). In SWAN, the wind input term and the whitecapping dissipation term are based on Komen et al. [24] formulation, improved by Rogers et al. [25] (referred to as ST1 hereafter). The dissipation parameterization in ST1 is based on the pulse-based model of Hasselmann [26], which is fundamentally different from that used in ST4 of WW3. For the computation of wind input

term, the drag coefficient formula from Wu [27] is used and it is capped at 0.0020 [28,29]. The DIA method is used to approximate the nonlinear interaction term. Details about settings of parameters associated with each source term are listed in Table 1. The setup of both models are commonly used [3,9,18,28].

## 2.2. Specification of Winds in Idealized Hurricanes

### 2.2.1. Idealized TC Wind Fields

The idealized TC wind fields are specified based on the parametric wind model of Holland [30]. The tangential wind speed  $V$  is computed as a gradient wind outside the radius of maximum wind ( $R_{max}$ ) and as a cyclostrophic winds inside  $R_{max}$ ,

$$V(r) = \begin{cases} \left( \frac{AB(P_n - P_c)}{\rho r^B} e^{-A/r^B} \right)^{1/2} & 0 \leq r \leq R_{max} \\ \left( \frac{AB(P_n - P_c)}{\rho r^B} e^{-A/r^B} + \frac{r^2 f^2}{4} \right)^{1/2} - \frac{rf}{2} & r > R_{max} \end{cases} \quad (1)$$

with,

$$B = \frac{\rho e V_{max}^2}{P_n - P_c} \quad (2)$$

$$A = R_{max}^B.$$

Here,  $r$  is radial distance from the storm center. The basic TC parameters involved are maximum wind speed ( $V_{max}$ ), radius of maximum wind ( $R_{max}$ ), central pressure ( $P_c$ , in pascal), environmental pressure ( $P_n$ , in pascal) and two constant coefficients  $A$  and  $B$ , as well as air density  $\rho$  (assumed constant at  $1.15 \text{ kg/m}^3$ ) and the Coriolis parameter  $f$ . For the idealized TC winds, the value of  $B$  is set to 2.0.

For idealized TCs, we prescribed three translation speeds (3 m/s, 6 m/s and 9 m/s) and two radii of maximum wind (25 km and 50 km). The maximum wind speed for all six idealized TCs is set to 50 m/s. In Table 2, these idealized storm parameters are compared with the storm parameters of a historical storm, known as the 1938 New England Hurricane (referred to as Hurricane 1938 hereafter), from 18 September to 22 September (landfall).

**Table 1.** Numerical and physical settings used in WW3 and SWAN.

Model Settings	WW3	SWAN
Numerics		
Time Step*	4 fractional time steps	1 global time step
Propagation Scheme	Third-order Ultimate Quickest (UQ) scheme	First Order, backward space, backward time (BSBT) scheme
Physics		
$S_{in} + S_{wc}$	ST4 (Ardhuin et al.)	ST1 (Komen)
	$z_{0_{max}} = 1.002, \beta_{max} = 1.43$	$C_{d_{max}} = 0.002$
$S_{nl}$		DIA (as default)

\* details on specific time step value are listed in Table 3.

**Table 2.** Characteristics of idealized storms and Hurricane 1938 between 18 September and 22 September.

TC Parameters	Idealized Storms	Hurricane 1938
Radius of Maximum Wind ( $R_{max}$ )	25 km (small), 50 km (large)	21~72 km (32.5 km on average)
Translation Speed ( $U_T$ )	3 m/s (slow), 6 m/s (medium), 9 m/s (fast)	5.6~21.6 m/s (12 m/s on average)
Maximum Winds ( $V_{max}$ )	50 m/s	31~72 m/s (62 m/s on average)

The final wind fields were then constructed by adding the inflow angles and the effects of translation speed following Moon et al. [31]. The inflow angles create cross-isobar (ageostrophic) wind component and the translation speed imposes asymmetry to the axisymmetric tropical cyclone vortex.

### 2.2.2. Specification of Winds in the Historic Hurricane

In addition to the idealized hurricanes, we also simulated the historic 1938 New England Hurricane. It is the most powerful hurricane in the recorded history that affected the Southern New England, causing property losses estimated at \$400 million at that time [32]. The storm made landfall in Long Island on 21 September 1939 as a Category 3 hurricane (storm characteristics are listed in Table 2). Before making landfall, its forward speed experienced dramatic increase and reached 70 mph (~30 m/s) [32,33]. Because its northward translation direction happened to align with the wind direction to the east of the storm, the fast forward speed increased the right-quadrant wind speeds far more than in a typical hurricane.

The parametric hurricane wind is generated using parameters reported in the best track files obtained from the NOAA National Hurricane Center (NHC) North Atlantic Hurricane database (HURDAT2) [33]. This is a re-analyzed best track database covering years from 1851 to 2016. The track files for historical storms only include the storm center position, maximum wind speed and central pressure. For Hurricane 1938, the central pressure information is unavailable for most of the storm period.

We have utilized the six available records of central pressure and have estimated the missing central pressure information by relating pressure deficit ( $P_n - P_c$ ) to the maximum wind speed squared ( $V_{max}^2$ ) through linear best fit according to Equation (2). Two assumptions were made. First, environmental pressure was assumed to be 1010 hPa. Second, we assumed a linear relation between the maximum wind speed squared and pressure deficit. This assumption seems reasonable for maximum wind speed between 60 and 140 knots (Figure 6b in Knaff and Zehr [34]). The maximum pressure drop estimated is 104 hPa with the corresponding maximum wind speed of 71.4 m/s. Since Knaff and Zehr [34] proposed to use storm-relative maximum wind for wind-pressure relationship, we also estimated the pressure deficit using the storm-relative maximum wind speed and confirmed that the pressure drop estimated in these two ways are similar (not shown).  $R_{max}$  was then calculated using the empirical formula suggested in Vickery et al. [35],

$$\ln R_{max} = 2.636 - 0.00005086\Delta p^2 + 0.0394899\psi \tag{3}$$

where  $\Delta p$  is the central pressure deficit (in hectopascal) and  $\psi$  is latitude of storm center (in degree). This formulation was derived from historical data for hurricane wind simulations in the Atlantic Basin, especially for storms located north of 30° N. As in the idealized experiments, the final wind fields were constructed by adding the inflow angles and the translation speeds. The characteristics of Hurricane 1938 during its life span is shown in Figure 2.

### 2.3. Experimental Design

We conducted experiments with four different spatial resolutions  $1/3^\circ$ ,  $1/6^\circ$ ,  $1/12^\circ$  and  $1/24^\circ$  for six idealized hurricanes (listed in Table 2) moving in four different directions, as shown in Figure 3. The purpose of simulating different storm translation directions is to investigate whether the results are affected by the direction of storm movement relative to the grid point locations. The computational domain size is set to  $30^\circ$  long in longitudinal direction and  $26^\circ$  wide in latitudinal direction. In all idealized experiments, the initial storm center was positioned  $2^\circ$  from the right and  $8^\circ$  from the bottom edge of the computational domain. This setting ensures enough domain space for simulation of the 9 m/s translating TC and avoids potential spurious effects caused by staying too close to the domain boundary. The water depth is horizontally uniform and set to 4000 m. The input wind field was constructed at the highest  $1/24^\circ$  resolution grid. In the low resolution grids, the wind vectors were identical to the highest resolution grid at the common grid points. No spatial interpolation of the wind field was done between different grid resolutions. The input wind was updated every 15 min in the model. A higher wind input frequency of 5 min was tested and the differences in the results were found to be insignificant. Depending on the translation speed of TCs, both wave models were integrated for 72 h (3 m/s) or 78 h (6 and 9 m/s) to ensure the wave field reaches quasi-steady state.

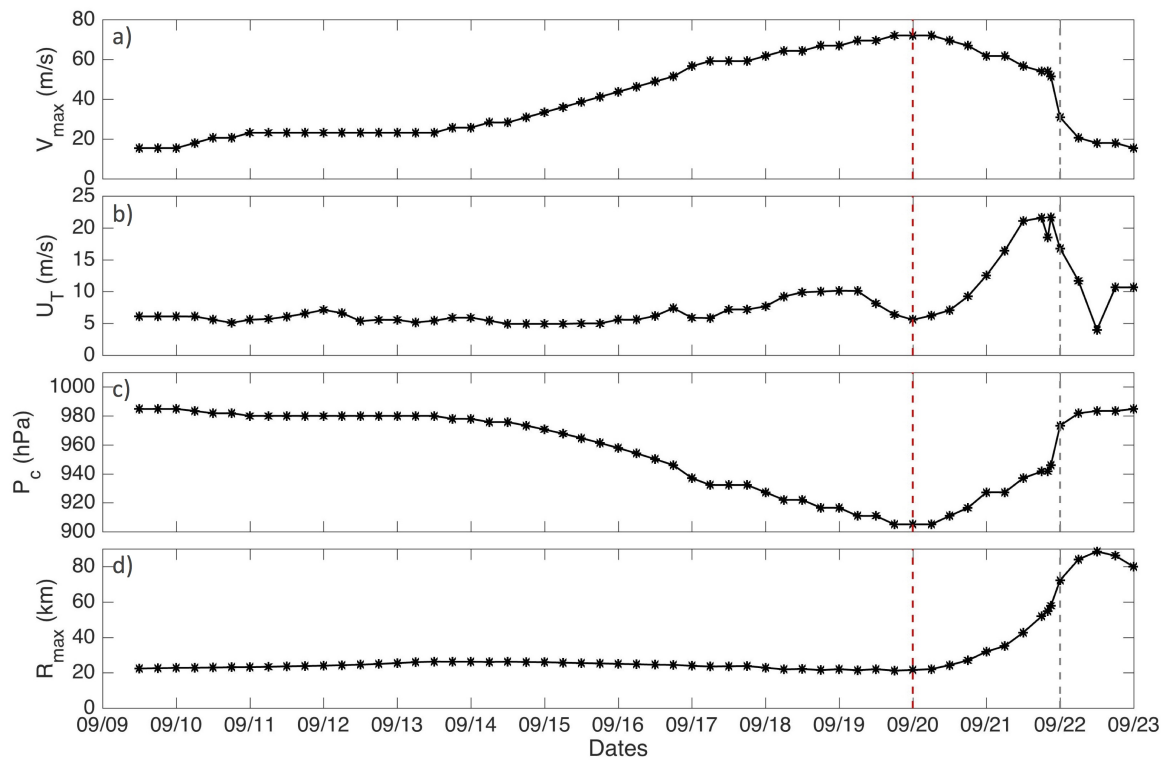


**Figure 2.** Characteristics of the 1938 New England Hurricane from 9 September 1938 to 23 September 1938. Panels (a–d) shows maximum wind speed ( $V_{max}$ ), translation speed ( $U_T$ ), central pressure ( $P_c$ ) and radius of maximum wind ( $R_{max}$ ), respectively. The latter two quantities are estimated. Red dashed line indicates the time when the hurricane is most intense (indicated by a minimum in central pressure); grey dashed line indicates the time of landfall in Rhode Island.

To solve the multi-timescale wave balance equation, WW3 applies a fractional step method that utilizes four different time steps: the global time step ( $\Delta t_{gmax}$ ), time steps for spatial propagation ( $\Delta t_{xy_{max}}$ ) and directional propagation ( $\Delta t_{\theta_{max}}$ ), and a time step for the source term integration ( $\Delta t_{src_{min}}$ ) [19]. Note that the spatial and directional propagation time steps are constrained by the Courant–Friedrichs–Lewy (CFL) condition. SWAN implements a different technique using

an action density limiter to restrict the rate of change of the energy spectrum at each time step [20]. Therefore, only one global time step is used. The specific settings of the time steps in both models are listed in Table 3.

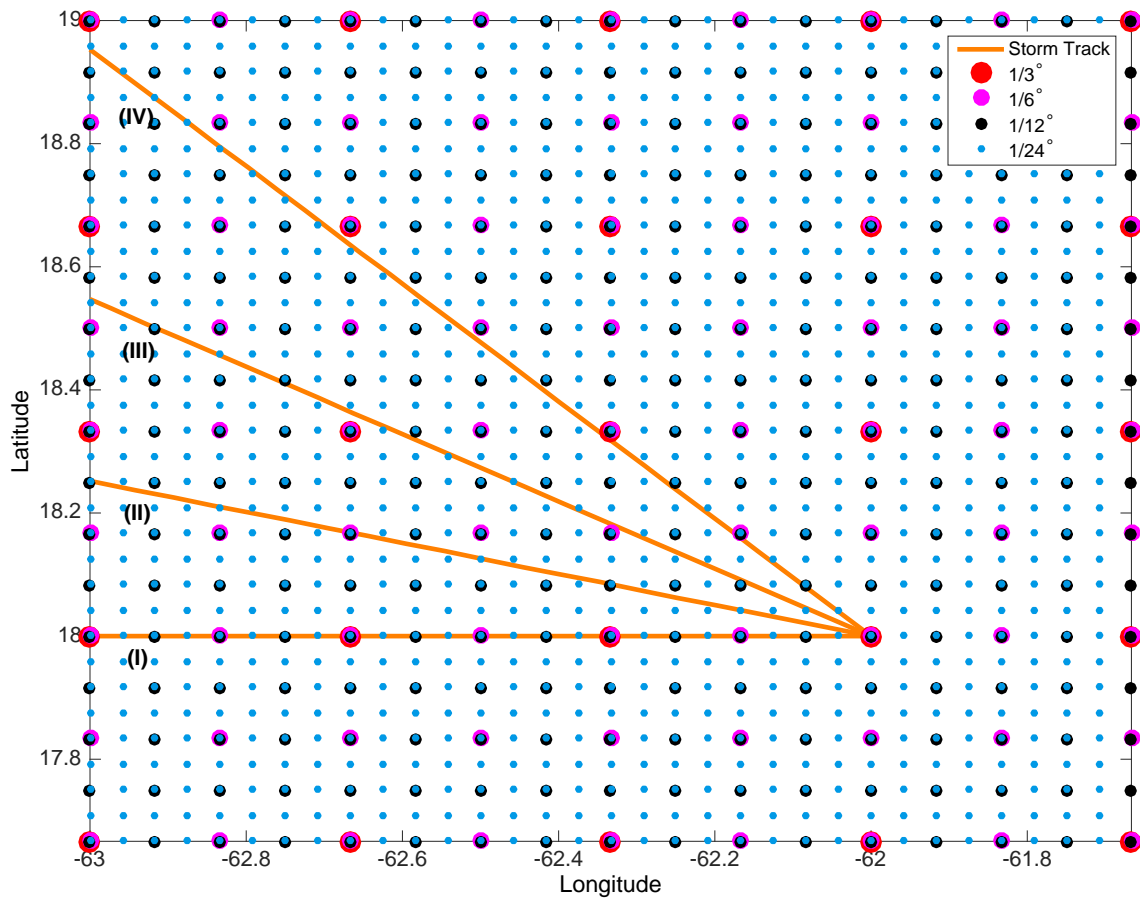


**Figure 3.** Configuration of model grids of different resolutions and storm tracks are shown in the southeast part of the computational domain. The storm tracks in four different directions are shown in orange. Size and color of the grid points denote the resolution. Red, magenta, black and cyan represent grid points in  $1/3^\circ$ ,  $1/6^\circ$ ,  $1/12^\circ$  and  $1/24^\circ$  resolutions, respectively. The angle of tracks are  $180^\circ$ ,  $165^\circ$ ,  $150^\circ$ , and  $135^\circ$  ( $0^\circ$  at positive  $x$ -axis).

**Table 3.** Spatial resolutions and corresponding numerical time steps set in two models.

Spatial Resolution	WW3			SWAN	
	$\Delta t_{g_{max}}$	$\Delta t_{xy_{max}}$	$\Delta t_{\theta_{max}}$	$\Delta t_{src_{min}}$	$\Delta t$
$1/3^\circ$					
$1/6^\circ$	300 s	237 s	118 s	30 s	300 s
$1/12^\circ$					
$1/24^\circ$		118 s	59 s		

The wave simulations for Hurricane 1938 were performed with  $1/3^\circ$  and  $1/12^\circ$  grid resolutions in a computational domain covering  $85^\circ$  W to  $55^\circ$  W and  $10^\circ$  N to  $45^\circ$  N. The model bathymetry was specified using the ETOPO1 1 arc-minute global Relief Model developed by the U.S. National Geophysical Data Center (NGDC) and spatially interpolated onto the given grid resolutions in Table 3.

### 3. Results

#### 3.1. Idealized Tropical Cyclone Wave Simulations

Results of the idealized TC experiments with both WW3 and SWAN models are presented in terms of five different quantities in a time-averaged quasi-steady wave field, namely, the maximum significant wave height (SWH), the spatial distribution of SWH, the (half-annulus) averaged wave energy, the spatial distribution of mean wavelength, and the time series of SWH at virtual buoys.

The time-averaged quasi-steady wave field was obtained by averaging hourly-output TC wave fields in a storm-following reference frame, over the last 24 h in quasi-steady state. Before time averaging, every instantaneous model output from a coarser resolution case was interpolated onto the  $1/24^\circ$  resolution grid points, which were used as the common grid points for comparing the results. The aforementioned five quantities were then obtained from this time-averaged wave field to remove potential numerical fluctuations due to a coarse resolution. Obtaining the SWH time series from this averaged wave field deserves some explanation. Because space and time are equivalent for the quasi-steady state wave field, a SWH time series is essentially a transect taken from the time averaged wave field in  $x$  direction at certain distance from the TC center. In the following analyses, we used the  $1/24^\circ$  resolution results as our benchmark results (i.e., the most accurate results), and used the terms “overestimation” and “underestimation” to describe the model results with coarser resolutions in comparison to the benchmark cases.

##### 3.1.1. Comparison of Maximum Significant Wave Heights

Figure 4 shows the maximum SWH from all simulations, with two different wave models, with six different idealized storms, with four different resolutions, and with four different storm propagation directions. As expected, larger and faster moving storms generate larger waves and hence higher values of maximum SWH. Varying spatial resolution in wave models as well as storm track direction affects the maximum SWH simulations. In general, for a fixed translation direction, as the storm moves faster, the  $1/3^\circ$  resolution tends to underestimate the maximum SWH. The largest errors of the maximum SWH reaches 1 m (about 6%) in WW3 and 2 m (about 16%) in SWAN with the  $1/3^\circ$  resolution. For a fixed resolution, the maximum SWH displays variability introduced by TC translation direction. In both models, this variability is reduced and the SWH results converge as the spatial resolution becomes finer. However, this convergence is slower in SWAN than that in WW3. Figure 4 also informs that, in both models, the variability caused by TC translation direction is comparable to the errors due to model resolution. Only with the  $1/3^\circ$  grid resolution and under the storm with a small  $R_{max}$  (large wind gradient) and a large translation speed (fast moving), the variation of SWH due to TC direction becomes significant. This is again more evident in SWAN.

In summary, model errors in maximum SWH (see Table 4) can be significant with coarser resolutions under a small and fast moving storm ( $R_{max} = 25$  km,  $U_T = 9$  m/s), using SWAN in particular. The sensitivity of maximum SWH to spatial resolution is model dependent and there are no systematic trends that are common in both models. This model dependency may be partly caused by the differences in their source terms. We have conducted the same experiments with WW3 but changed the source terms from ST4 to ST2 (Tolman and Chalikov [36]), and found different sensitivity to the spatial resolution (not shown).

##### 3.1.2. Comparison of Spatial Distribution of Significant Wave Heights

In terms of practical interest, it is also important to compare spatial distribution of SWH in hurricanes simulated at different spatial resolutions, which is not represented by the previous comparison of maximum SWH. For simplicity, only the results generated by horizontally-moving storms are presented hereafter.

In Figures 5 and 6, the SWH fields simulated with the  $1/3^\circ$  and  $1/24^\circ$  grids are compared in a domain of  $4R_{max}$  by  $4R_{max}$  around the storm center. The difference between the two is shown in the right column.

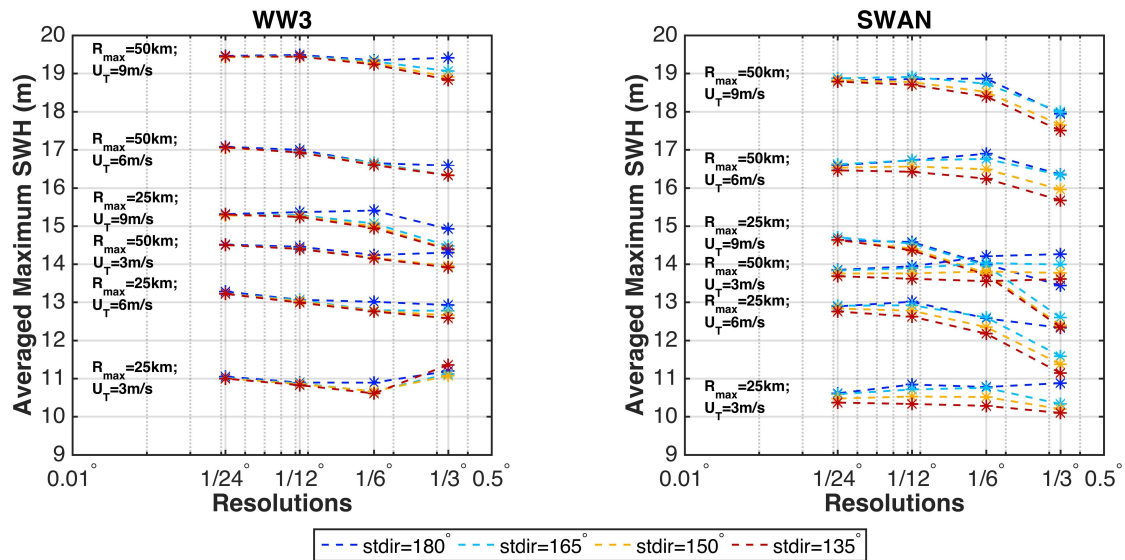


**Figure 4.** Maximum SWH in time-averaged quasi-steady state wave fields simulated with six different idealized storms, with four different spatial resolutions, and with four different storm propagation directions: (a) WW3 results; and (b) SWAN results. Dashed lines of different colors represent different directions, with track (I) in blue, track (II) in cyan, track (III) in yellow and track (IV) in red. Asterisk marker denotes the actual data point.

**Table 4.** Largest absolute errors in maximum SWH with different resolutions relative to results with the highest resolution ( $1/24^\circ$ ).

$R_{max}$ (km)	$U_T$ (m/s)	$1/3^\circ$		$1/6^\circ$		$1/12^\circ$	
		WW3	SWAN	WW3	SWAN	WW3	SWAN
25	3	3.3%	2.6%	3.5%	1.6%	1.6%	2.2%
	6	4.8%	12.6%	3.5%	4.6%	1.7%	1.1%
	9	6.0%	15.7%	2.3%	6.3%	0.4%	1.9%
50	3	4.1%	3.0%	2.4%	2.6%	0.7%	0.7%
	6	4.3%	4.8%	2.7%	1.8%	0.8%	0.8%
	9	3.2%	6.8%	1.1%	2.1%	0.1%	0.4%

In WW3 (Figure 5), the coarse resolution results with slow moving (3 m/s) storms significantly overestimate the small SWH near the storm center inside  $R_{max}$  but the errors are relatively small outside  $R_{max}$ . For fast moving storms (9 m/s), this overestimation near the storm center is reduced, but SWH in front of the storm near  $R_{max}$  is underestimated (as much as 17%), and SWH further in front and further behind are overestimated (as much as 50%) with the coarse resolution. The overall errors in SWH appear to be the largest for smaller and faster moving storms with coarser model resolutions.

In SWAN (Figure 6), the overall error patterns are qualitatively similar to those in WW3. However, the underestimation of SWH with the coarser resolution in front of the storm is more significant (23%) and affects a larger area in the fast moving storms. The overestimation of SWH (27%) further in front of the storm (within  $4R_{max}$ ) tends to be smaller in comparison to WW3.

In summary, in both models, the spatial distribution of SWH appears to be most sensitive to the model spatial resolution for small ( $R_{max} = 25$  km) and fast moving ( $U_T = 9$  m/s) hurricanes, with the error magnitude exceeding 2.5 m in some locations.

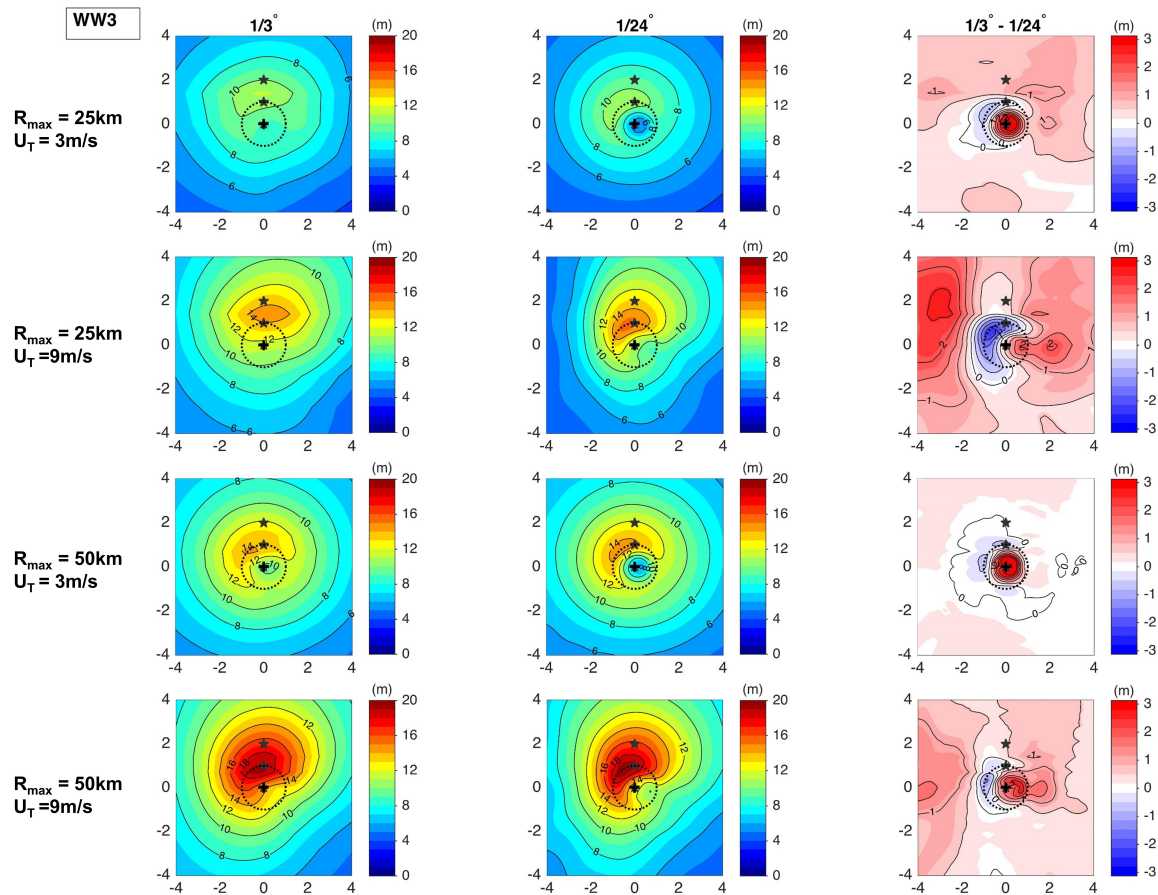


**Figure 5.** Spatial distribution of SWH in time-averaged quasi-steady state wave fields from WW3. The results computed: at  $1/3^\circ$  resolution (**left**); and at  $1/24^\circ$  resolution (**right**). The black contours have an increment of 3 m. The differences between the left and center columns, and the black contours are drawn every 0.5 m (**right**). Distances are normalized by  $R_{max}$ . The black dotted circle denotes  $R_{max}$ . Filled black stars on each panel denote the location of virtual buoys discussed in Section 3.1.5.

### 3.1.3. Comparison of Half-Annulus Averaged Wave Energy

Our analysis in the previous section suggests that the errors in SWH due to the coarse model resolution vary with the distance from the storm center, as well as whether the location is in front or behind the storm center. Here, we explore the model errors further by comparing the averaged wave energy in front and behind the storm center. By definition, the square of SWH is proportional to the total wave energy per unit surface area, integrated over the entire directional spectrum in the model. Here, we compare the half-annulus averaged wave energy in the front and rear halves of the storm (relative to the storm center). Specifically, we draw a series of circles, with their radii ranging from 0 to  $5R_{max}$  with an increment of  $0.2R_{max}$ , and define a series of annuli between the two successive circles. We further divide each annulus into front half and rear half, and compute the average wave energy in each half-annulus region.

Figures 7 and 8 show the half-annulus averaged wave energy computed in this manner in all the simulations with WW3 and SWAN, respectively. The averaged wave energy is always higher in the front half (negative normalized distance) than in the rear half (positive normalized distance) of the storm. This asymmetry is more significant in large and fast moving storms. The wave energy peaks

near  $R_{max}$  are not well resolved with the  $1/3^\circ$  resolution in both models, especially for the small storms. The coarse resolution simulations overestimate the wave energy near the storm center in most cases (except the small fast moving storm with SWAN). The overestimation of wave energy in the far field with the  $1/3^\circ$  resolution (in WW3 only) is also noticeable. In small storms, the cumulative wave energy within a  $5R_{max}$  circular area is about 20% higher in the  $1/3^\circ$  simulation than in the  $1/24^\circ$  simulation. Spatially, there are no systematic biases in the wave energy errors due to the coarse resolutions, which suggests these errors cannot be mitigated empirically. Moreover, the model sensitivity to the grid resolution in the front of the storm is very different from that behind the storm. These results suggest that projecting the high resolution TC wind field on the coarse resolution grid, which would smooth the wind field and reduce wind input both near the front peak and near the rear peak, is not the only reason for the errors in the wave simulations. The result from an additional sensitivity experiment, where a spatially smoothed wind field at  $1/3^\circ$  grid resolution is used to force WW3 at the highest spatial resolution, further confirms this argument (see Appendix A).

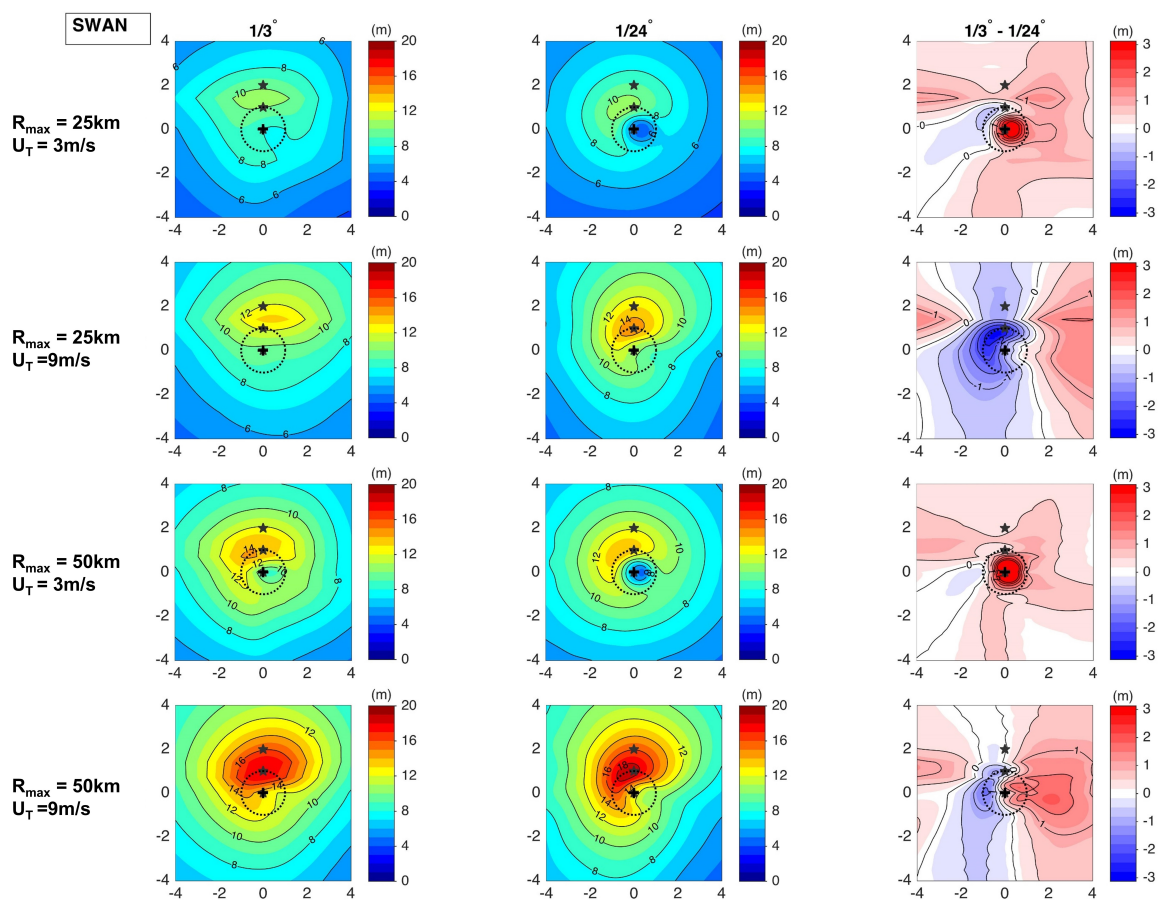


**Figure 6.** Spatial distribution of SWH in time-averaged quasi-steady state wave fields from SWAN. The results computed: at  $1/3^\circ$  resolution (**left**); and at  $1/24^\circ$  resolution (**right**). The figure format is the same as in Figure 5.

### 3.1.4. Comparison of Spatial Distribution of Mean Wavelength

We next investigated how the simulated mean wavelength (MWL) is affected by the different model resolutions. Unfortunately, there is no common definition of the mean wavelength shared by WW3 and SWAN. In WW3, MWL is defined as the wavelength weighted averaged by spectral density. In SWAN, MWL is defined as the wavelength associated with the mean wavenumber (MWN), which is the wavenumber weighted averaged by spectral density. These different definitions partially explain the different spatial patterns of MWL seen in Figures 9 and 10.

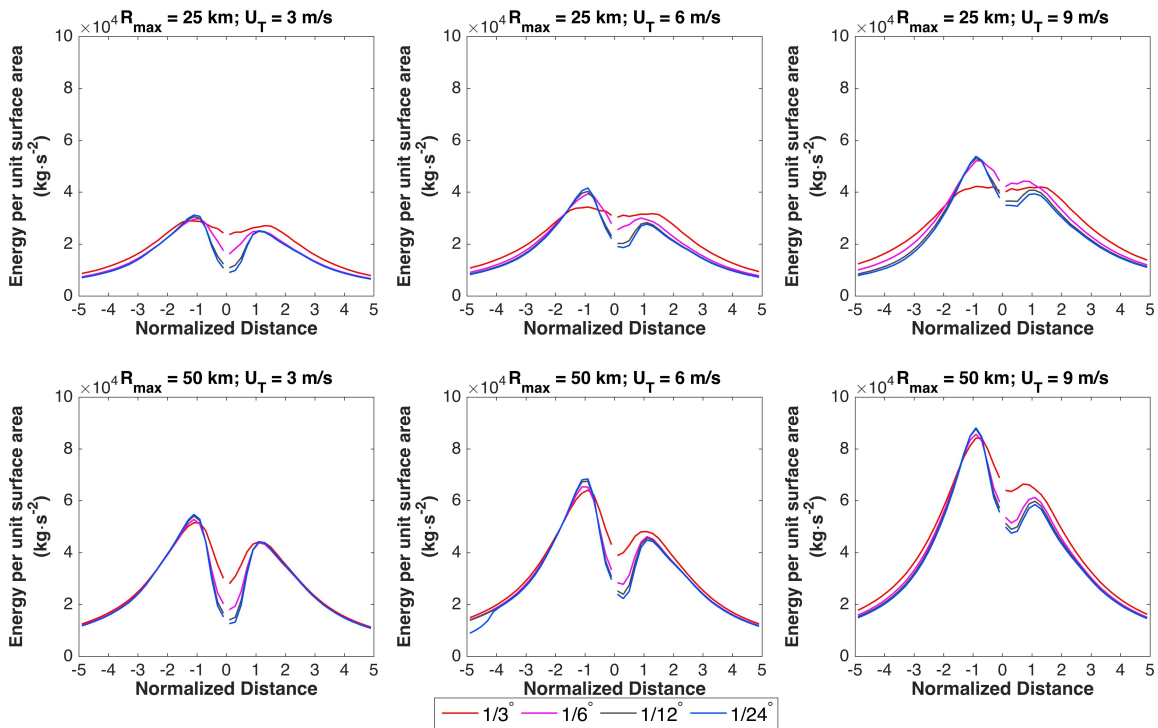


**Figure 7.** Average wave energy within a half-annulus area (front and rear) at different radii from the storm center under the six idealized storms from WW3. Red, magenta, black and blue lines denote results from the coarsest to the highest resolution.

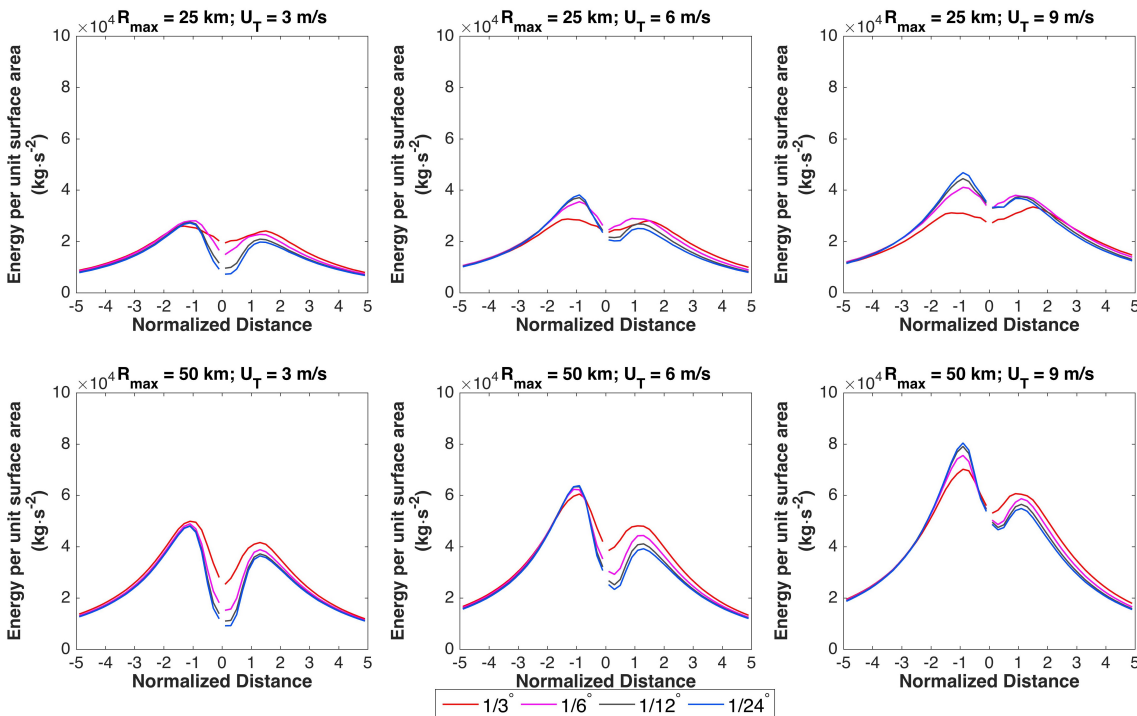


**Figure 8.** Average wave energy within a half-annulus area (front and rear) at different radii from the storm center under the six idealized storms from SWAN. Red, magenta, black and blue lines denote results from the coarsest to the highest resolution.

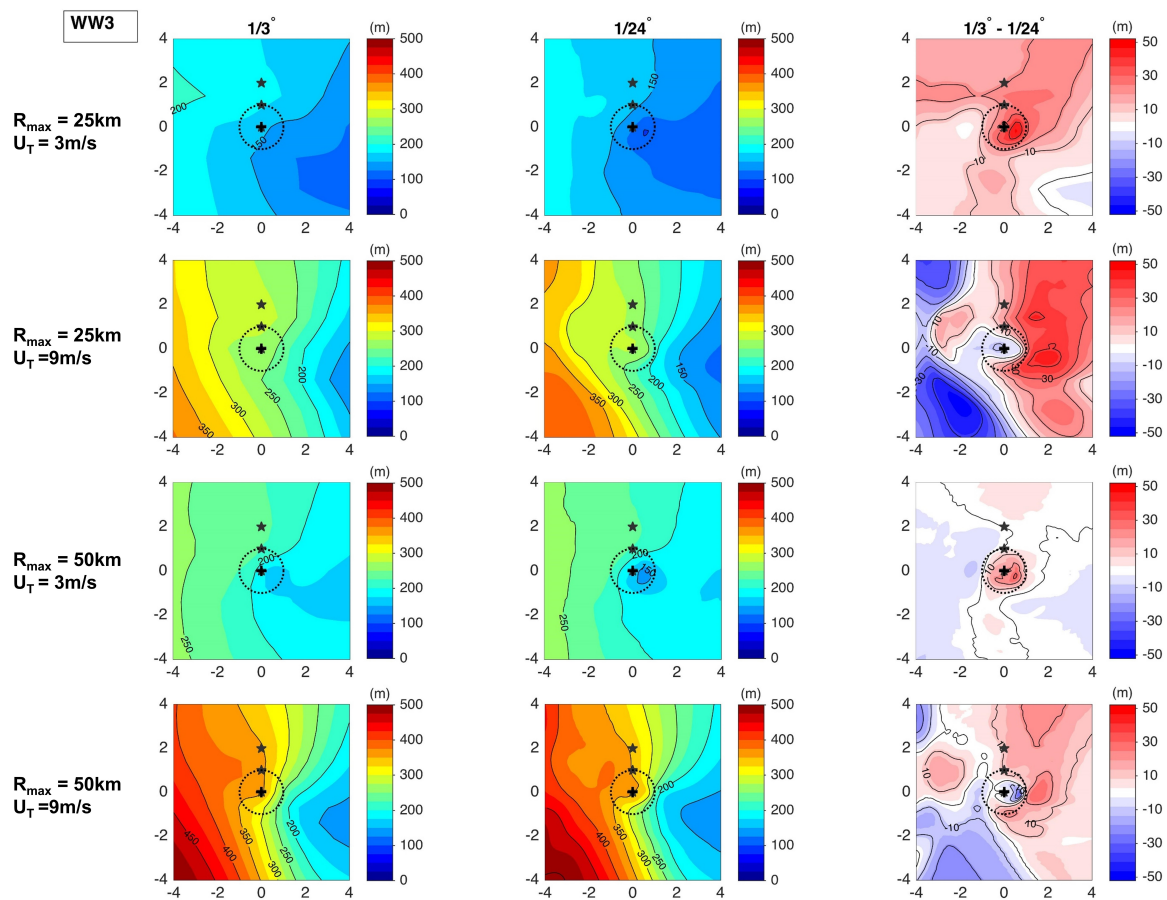


**Figure 9.** Spatial distribution of mean wavelength (wavelength weighted averaged by spectral density) in time-averaged quasi-steady state wave fields from WW3. The figure format is the same as Figure 5.

Figure 9 shows that MWL in WW3 monotonically increases in the direction of storm propagation, in general. This is because only longer swells can propagate ahead of the storm. The MWL errors in the  $1/3^\circ$  resolution are as large as 50 m in the small and fast moving storm. The overall effect of a coarse grid is underestimation of the wavelength of swells ahead of the storm and overestimation of the wavelength of wind seas within the storm.

In SWAN, the presence of long swells ahead of storms have a smaller contribution to its MWL by definition, because MWN is not dominated by long swells. Therefore, the characteristic wavelength ahead of the storm in Figure 10 is significantly shorter than the one in Figure 9. Nevertheless, the errors due to the coarse resolution are as large as 50 m in some cases/locations for this characteristic wavelength.

### 3.1.5. Comparison of SWH at Virtual Buoys

To further assess impacts of different model spatial resolutions, we compared the SWH time series at select locations, hereafter “virtual buoys”. We deployed three virtual buoys at the storm center, at the  $R_{max}$  and  $2R_{max}$  to the right of the storm center (locations shown in Figures 5 and 6). Figure 11 shows the SWH time series under the small and fast moving storm at these three buoys in both WW3 and SWAN.

The results from both wave models show similar impacts of the coarse resolutions, especially  $1/3^\circ$ . Firstly, the duration of SWH exceeding a certain magnitude, e.g., 4 m, is extended with the coarse resolutions, because SWH further away from the storm are overestimated. Secondly, the arrival time of the highest SWH is delayed by up to 0.5~1 h at all three buoys. Thirdly, the maximum SWH is significantly underestimated at the two buoys closer to the storm center. These virtual buoy records

are consistent with the previously discussed SWH spatial maps for different resolutions. They confirm that the  $1/3^\circ$  resolution simulations are not capable of accurately simulating the structure of the TC wave field.

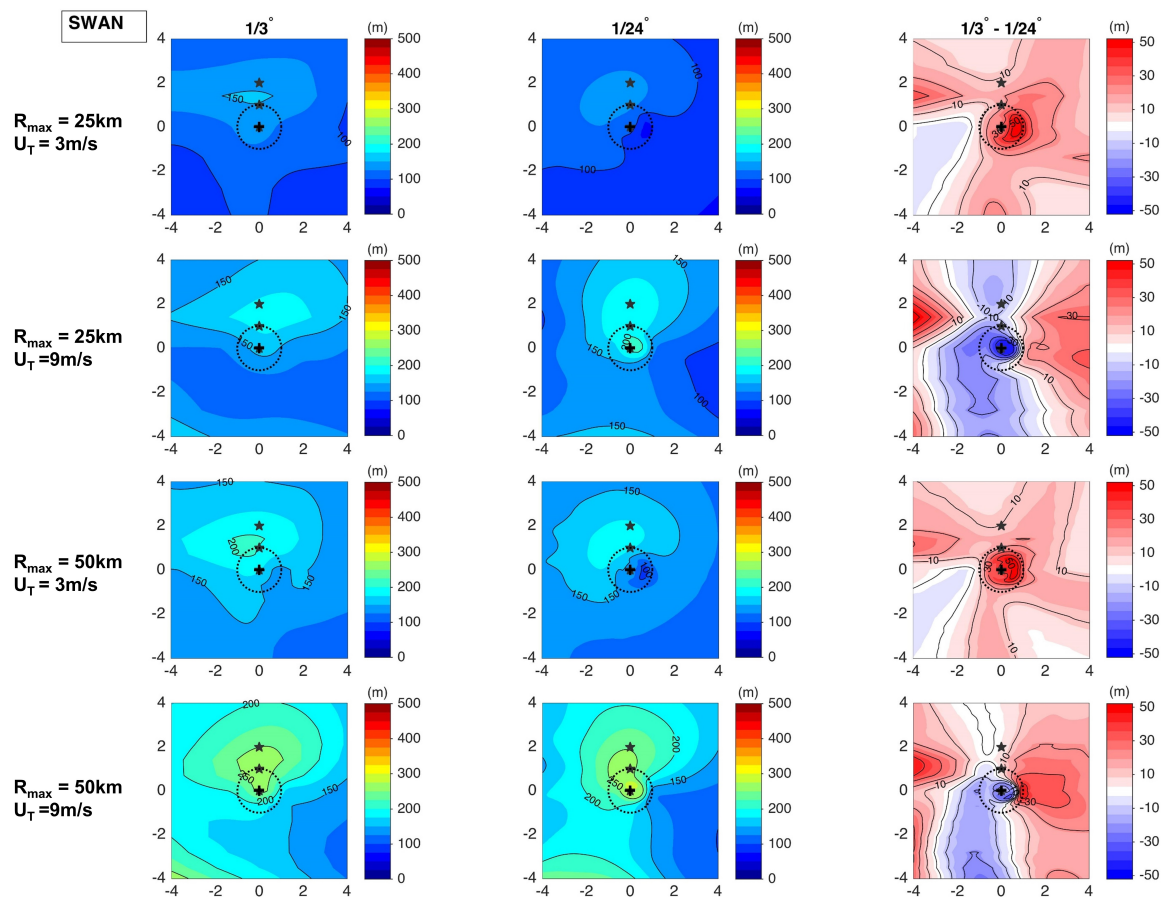


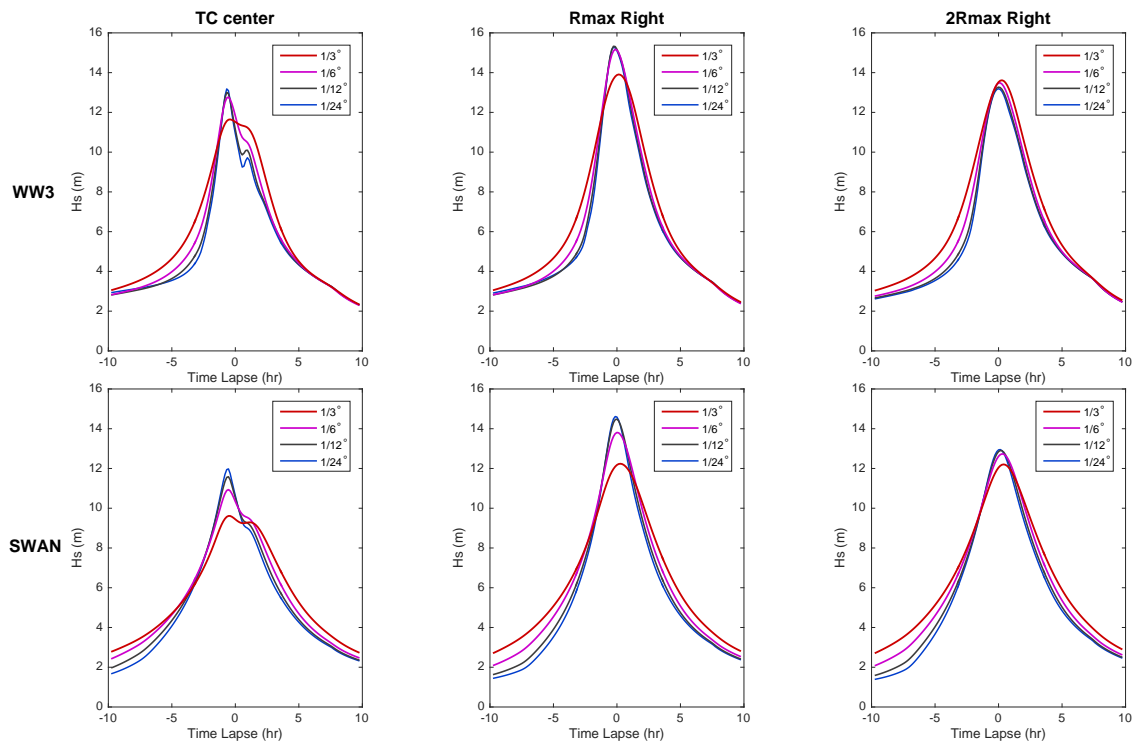
**Figure 10.** Spatial distribution of wavelength corresponding to mean wavenumber (wavenumber weighted averaged by spectral density) in time-averaged quasi-steady state wave fields from SWAN. The figure format is the same as Figure 5.

### 3.2. Wave Simulations under the 1938 New England Hurricane

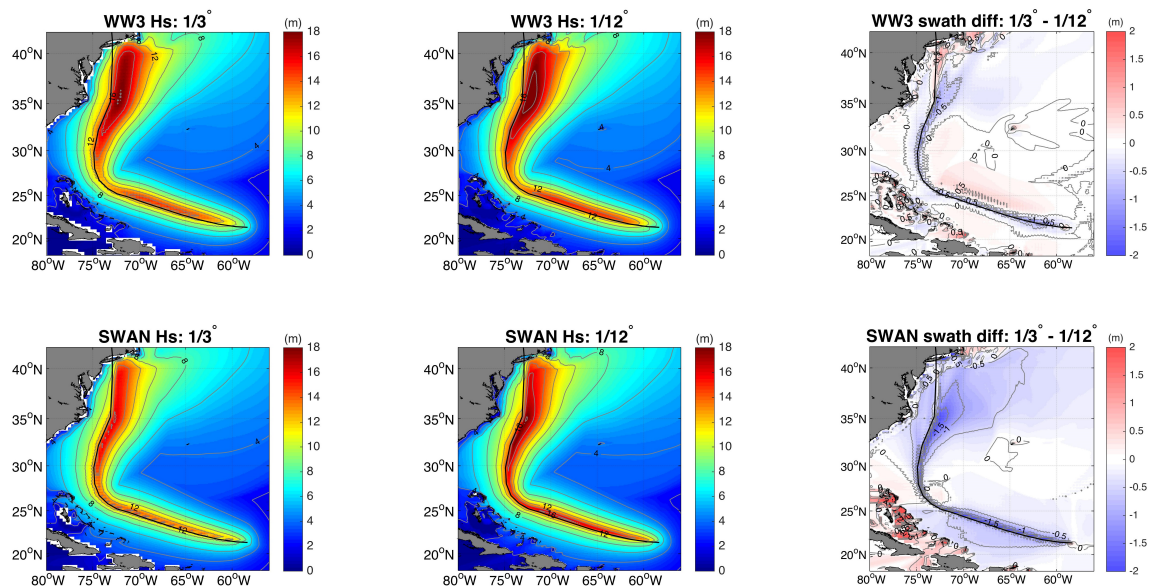
To examine if our findings from the above idealized experiments are applicable to real TCs, wave simulations with different spatial resolutions are performed for the 1938 New England Hurricane. This hurricane is chosen because its  $R_{max}$  remained relatively small for a long period of time offshore and it had an unusually fast translation speed (see Figure 2).

Figure 12 shows the swaths of maximum SWH with two different resolutions,  $1/3^\circ$  (left column) and  $1/12^\circ$  (center column), using WW3 (top row) and SWAN (bottom row). These swaths are constructed by finding the maximum value of the SWH time series during the storm passage at each grid point.

The largest waves are generated near the Cape Hatteras around  $35^\circ$  N. From the swath difference shown in the right columns, we notice that the maximum waves are underestimated in the  $1/3^\circ$  simulation by up to 1 m (5.3%) in WW3 and up to 1.5 m (8.3%) in SWAN. The degree of underestimation in the peak waves with the coarse resolution is consistent with what we have found in the idealized experiments. To summarize, this real case simulation further confirms that using the  $1/3^\circ$  spatial resolution can lead to significant errors in wave predictions under a small and fast moving TC.



**Figure 11.** Time series of SWH at three virtual buoys (locations shown in Figures 5 and 6) under the small ( $RMW = 25$  km) and fast moving ( $U_T = 9$  m/s) storm: from WW3 (top row); and from SWAN (bottom row). SWH time series recorded at : storm center (left column);  $R_{max}$  to the right of storm center (center column); and  $2R_{max}$  to the right of storm center (right column). Red, magenta, black and blue lines denote results from the coarsest to the finest resolution.



**Figure 12.** Comparison of swath of maximum SWH: in a  $1/3^\circ$  simulation (left column); and in a  $1/12^\circ$  simulation (center column); and their difference (right column), under Hurricane 1938. (top row) WW3 results; and (bottom row) SWAN results. Hurricane track is denoted by the black solid line. Contour increment for swath is 3 m. Contour increment for swath difference is 0.5 m.

#### 4. Conclusions and Discussion

We conducted the first modeling study quantifying the sensitivity of TC wave simulations to spatial resolutions in open ocean. Based on the results from a series of idealized experiments with two widely used wave models, WW3 and SWAN, main conclusions can be summarized as follows.

1. Wave model sensitivity to spatial resolution depends on storm characteristics. Waves generated under a small and fast moving storm ( $R_{max} = 25$  km,  $U_T = 9$  m/s in this study) appear to be most sensitive to a coarse resolution.
2. Under a small and fast moving storm, using the  $1/3^\circ$  spatial resolution can lead to underestimation of the maximum SWH by 6% in WW3(ST4) and 16% in SWAN(ST1). The local SWH in front of the storm near  $R_{max}$  can be underestimated by as much as 17% in WW3 and 23% in SWAN.
3. In all six idealized storms, the coarsest resolution of  $1/3^\circ$  causes the largest errors in both SWH and MWL. In general, the sensitivity to model spatial resolution is larger in SWAN(ST1) than that in WW3(ST4).
4. The errors due to spatial resolution are comparable to those due to different physics parameterizations in wave models, which are on the order of 5~10% (Liu et al. [18]).

Based on our experimental results, the following recommendations can be made on the spatial resolution threshold required for different applications. For predictions of the maximum SWH with ~5% accuracy, a resolution higher than  $1/3^\circ$  is recommended for WW3(ST4), and a resolution higher than  $1/6^\circ$  is recommended for SWAN(ST1). However, to predict spatial patterns of TC waves within ~5% error, the spatial resolution has to be higher than  $1/6^\circ$  in both models (Table A1 in Appendix B and more details in the Supplementary Material). In the current NOAA WW3 operational hurricane wave model ( $1/10^\circ$  resolution), the model error due to spatial resolution is estimated to be less than 5%. In the ADCIRC-SWAN real-time guidance system [10], the mesh resolution over the open ocean needs to be refined to at least  $1/6^\circ$  to make the SWAN wave predictions reasonably accurate. Meanwhile, WW3(ST4) may be a better candidate for storm surge-wave coupling, since it is less sensitive to spatial resolution than SWAN(ST1).

Underestimating the peak of extreme waves under storms is a known limitation of the current third generation wave models [37,38]. Potential reasons have been discussed in [37] but the exact source of errors remains unknown. Although our study cannot provide an answer to this question, our results demonstrate that spatial smoothing of the wind field is not the only reason for the errors in wave simulations with coarse resolution grids (see Figure A1 in Appendix A).

To investigate further the sensitivity of TC wave simulations to other numerical settings in WW3 and SWAN, we performed the following additional tests: (1) higher temporal resolution of input wind (increased from 15 min to wave model time step); (2) higher directional resolution of the wave spectrum (increased from 24 bins to 36 bins); (3) higher model temporal resolution in SWAN (increased from 300 s to 120 s); and (4) reduction of splitting errors in WW3 due to four different time steps (set the four time steps to 30 s). In all of these experiments, changes in the maximum SWH predictions did not exceed 1%.

In conclusion, our study clearly demonstrates that a coarse spatial resolution such as  $1/3^\circ$  is not suitable for simulating TC waves, particularly in smaller and faster moving storms. The results of this study raise questions regarding the accuracy of TC wave simulations with unstructured grids in the coupled ADCIRC-SWAN or similar systems that use coarse spatial resolutions in the open ocean region and its impacts on storm surge predictions. In the coupled storm surge-wave system, one important quantity used to account for wave impacts on storm surge is the radiation stress, which is essentially the spatial gradient of the wave field. Although this quantity is more significant in the shallow water region, where the spatial resolution is typically high, the coarse resolution errors in the offshore region may still impact the results if the incoming waves are significantly underestimated. More careful

studies with different unstructured grid systems, including the coastal regions, are needed to fully examine the accuracy of the wave simulations and their impacts on storm surge.

**Supplementary Materials:** The following are available online at <http://www.mdpi.com/2077-1312/6/4/116/s1>.

**Author Contributions:** Conceptualization, T.H. and I.G.; Methodology, T.H. and X.C.; Software, X.C.; Validation, X.C.; Formal Analysis, X.C.; Investigation, X.C.; Resources, X.C.; Data Curation, X.C.; Writing—Original Draft Preparation, X.C.; Writing—Review and Editing, I.G. and T.H.; Visualization, X.C.; Supervision, I.G. and T.H.; Project Administration, I.G.; and Funding Acquisition, I.G.

**Funding:** This research was funded by U.S. Department of Homeland Security under Grant Award Number 2015-ST-061-ND0001-01.

**Acknowledgments:** The authors would like to acknowledge Jessica Meixner from the Environmental Modeling Center (EMC) at the National Centers for Environmental Prediction (NCEP) for providing information on the operational WAVEWATCH III. We also thank the anonymous reviewers for their valuable comments.

**Conflicts of Interest:** The authors declare no conflict of interest. The founding sponsors had no role in the design of the study; in the collection, analyses, or interpretation of data; in the writing of the manuscript, and in the decision to publish the results.

### Appendix A

To clarify further the effect of a smoothed wind field on the wave simulations, an additional sensitivity experiment was performed for the small and fast moving TC case using WW3. In this additional experiment, the wind field was generated at  $1/3^\circ$  spatial resolution but the wave model was run at  $1/24^\circ$  spatial resolution. Note this is exactly the same wind field as used to force the  $1/3^\circ$  WW3 experiments discussed above. In Figure A1, the result is compared to that of the original experiments where the prescribed winds are not smoothed. The smoothed input wind field in the  $1/24^\circ$  experiment (dashed line) lowers the wave energy in both front and rear region and retains the energy asymmetry. This additional test clearly demonstrates that smoothing of the wind field simply reduces the wave energy everywhere and does not change the energy distribution in the wave field, as shown in the low resolution experiments.

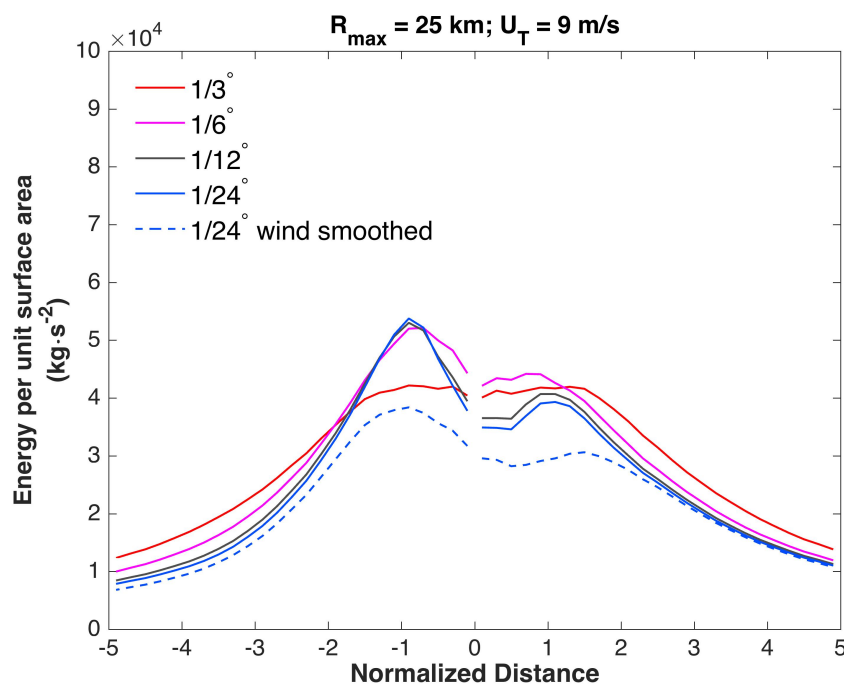


**Figure A1.** Comparison of the half-annulus averaged wave energy in original experiments (solid lines) and in an additional experiment forced by a smoothed wind field of  $1/3^\circ$  spatial resolution (dashed line).

## Appendix B

Maximum errors in local SWH in right front of the storm near  $R_{max}$  in  $1/3^\circ$ ,  $1/6^\circ$ , and  $1/12^\circ$  resolution simulations are provided below for reference. The ranges are produced by the variation of TC translation direction. Errors associated with each TC translation direction are documented in the Supplementary Material.

**Table A1.** Maximum underestimation of the local SWH at right front  $R_{max}$  with different resolutions relative to results with  $1/24^\circ$ .

$R_{max}$ (km)	$U_T$ (m/s)	$1/3^\circ$		$1/6^\circ$		$1/12^\circ$	
		WW3	SWAN	WW3	SWAN	WW3	SWAN
25	3	-10.5~0%	-9.8~-2.8%	-6.0~-3.6%	-2.9~-1.5%	-3.8~-1.6%	-1.9~-1.4%
	6	-15.7~-6.9%	-19.0~-11.7%	-6.9~-4.9%	-7.3~-6.2%	-3.8~-2.0%	-3.8~-2.2%
	9	-17.4~-8.7%	-22.9~-16.6%	-5.4~-4.7%	-8.9~-7.9%	-2.8~-1.4%	-4.2~-2.8%
50	3	-6.3~-4.3%	-3.3~-2.5%	-4.4~-2.5%	-3.3~-2.6%	-1.3~-0.9%	-2.0~-1.4%
	6	-8.4~-5.9%	-8.3~-6.5%	-5.3~-3.3%	-5.4~-3.9%	-2.2~-1.8%	-2.4~-1.7%
	9	-6.9~-5.8%	-11.1~-9.4%	-3.9~-2.4%	-7.3~-5.3%	-1.2~-0.9%	-3.2~-1.9%

## References

1. Barber, N.; Ursell, F. The generation and propagation of ocean waves and swell. I. Wave periods and velocities. *Philos. Trans. R. Soc. Lond. A* **1948**, *240*, 527–560. [[CrossRef](#)]
2. Longuet-Higgins, M.; Stewart, R. Radiation stresses in water waves; a physical discussion, with applications. *Deep Sea Res. Oceanogr. Abstr.* **1964**, *11*, 529–562. [[CrossRef](#)]
3. Dietrich, J.; Zijlema, M.; Westerink, J.; Holthuijsen, L.; Dawson, C.; Luettich, R.A.; Jensen, R.; Smith, J.; Stelling, G.; Stone, G. Modeling hurricane waves and storm surge using integrally-coupled, scalable computations. *Coast. Eng.* **2011**, *58*, 45–65. [[CrossRef](#)]
4. Sun, Y.; Chen, C.; Beardsley, R.C.; Xu, Q.; Qi, J.; Lin, H. Impact of current-wave interaction on storm surge simulation: A case study for Hurricane Bob. *J. Geophys. Res. Oceans* **2013**, *118*, 2685–2701. [[CrossRef](#)]
5. Feng, X.; Yin, B.; Yang, D. Development of an unstructured-grid wave-current coupled model and its application. *Ocean Model.* **2016**, *104*, 213–225. [[CrossRef](#)]
6. Donelan, M.A.; Curcic, M.; Chen, S.S.; Magnusson, A.K. Modeling waves and wind stress. *J. Geophys. Res. Oceans* **2012**, *117*. [[CrossRef](#)]
7. Reichl, B.G.; Hara, T.; Ginis, I. Sea state dependence of the wind stress over the ocean under hurricane winds. *J. Geophys. Res. Oceans* **2014**, *119*, 30–51. [[CrossRef](#)]
8. Bunya, S.; Dietrich, J.C.; Westerink, J.J.; Ebersole, B.A.; Smith, J.M.; Atkinson, J.H.; Jensen, R.; Resio, D.T.; Luettich, R.A.; Dawson, C.; et al. A High-Resolution Coupled Riverine Flow, Tide, Wind, Wind Wave, and Storm Surge Model for Southern Louisiana and Mississippi. Part I: Model Development and Validation. *Mon. Weather Rev.* **2010**, *138*, 345–377. [[CrossRef](#)]
9. Dietrich, J.C.; Bunya, S.; Westerink, J.J.; Ebersole, B.A.; Smith, J.M.; Atkinson, J.H.; Jensen, R.; Resio, D.T.; Luettich, R.A.; Dawson, C.; et al. A High-Resolution Coupled Riverine Flow, Tide, Wind, Wind Wave, and Storm Surge Model for Southern Louisiana and Mississippi. Part II: Synoptic Description and Analysis of Hurricanes Katrina and Rita. *Mon. Weather Rev.* **2010**, *138*, 378–404. [[CrossRef](#)]
10. Fleming, J.G.; Fulcher, C.W.; Luettich, R.A.; Estrade, B.D.; Allen, G.D.; Winer, H.S. A Real Time Storm Surge Forecasting System Using ADCIRC. In Proceedings of the 10th International Conference on Estuarine and Coastal Modeling, Newport, RI, USA, 5 November 2007; pp. 893–912.
11. Dresback, K.M.; Fleming, J.G.; Blanton, B.O.; Kaiser, C.; Gourley, J.J.; Tromble, E.M.; Luettich, R.A.; Kolar, R.L.; Hong, Y.; Cooten, S.V.; et al. Skill assessment of a real-time forecast system utilizing a coupled hydrologic and coastal hydrodynamic model during Hurricane Irene (2011). *Cont. Shelf Res.* **2013**, *71*, 78–94. [[CrossRef](#)]

12. Kerr, P.C.; Martyr, R.C.; Donahue, A.S.; Hope, M.E.; Westerink, J.J.; Luettich, R.A.; Kennedy, A.B.; Dietrich, J.C.; Dawson, C.; Westerink, H.J. U.S. IOOS coastal and ocean modeling testbed: Evaluation of tide, wave, and hurricane surge response sensitivities to mesh resolution and friction in the Gulf of Mexico. *J. Geophys. Res. Oceans* **2013**, *118*, 4633–4661. [[CrossRef](#)]
13. Xu, Y.; He, H.; Song, J.; Hou, Y.; Li, F.; Xu, Y.; He, H.; Song, J.; Hou, Y.; Li, F. Observations and Modeling of Typhoon Waves in the South China Sea. *J. Phys. Oceanogr.* **2017**, *47*, 1307–1324. [[CrossRef](#)]
14. Haiden, T.; Janousek, M.; Bidlot, J.; Ferranti, L.; Prates, F.; Vitart, F.; Bauer, P.; Richardson, D. *Evaluation of ECMWF Forecasts, Including the 2016 Resolution Upgrade*; European Centre for Medium-Range Weather Forecasts: Reading, UK, 2016.
15. Chawla, A.; Tolman, H.L.; Gerald, V.; Spindler, D.; Spindler, T.; Alves, J.H.G.M.; Cao, D.; Hanson, J.L.; Devaliere, E.M. A Multigrid Wave Forecasting Model: A New Paradigm in Operational Wave Forecasting. *Weather Forecast.* **2013**, *28*, 1057–1078. [[CrossRef](#)]
16. Shimura, T.; Mori, N.; Hemer, M.A. Projection of tropical cyclone-generated extreme wave climate based on CMIP5 multi-model ensemble in the Western North Pacific. *Clim. Dyn.* **2017**, *49*, 1449–1462. [[CrossRef](#)]
17. Tolman, H.L.; Alves, J.H.G. Numerical modeling of wind waves generated by tropical cyclones using moving grids. *Ocean Model.* **2005**, *9*, 305–323. [[CrossRef](#)]
18. Liu, Q.; Babanin, A.; Fan, Y.; Zieger, S.; Guan, C.; Moon, I.J. Numerical simulations of ocean surface waves under hurricane conditions: Assessment of existing model performance. *Ocean Model.* **2017**, *118*, 73–93. [[CrossRef](#)]
19. The WAVEWATCH III<sup>®</sup> Development Group. *User Manual and System Documentation of WAVEWATCH III<sup>®</sup> Version 5.16*; Tech. Note 329; NOAA/NWS/NCEP/MMAB: College Park, MD, USA, 2016.
20. The SWAN Team. *SWAN Scientific and Technical Documentation (Cycle III Version 41.10A)*; Technology Note, Version 41.10; Delft University of Technology: Delft, The Netherlands, 2012.
21. Fan, Y.; Ginis, I.; Hara, T.; Wright, C.W.; Walsh, E.J. Numerical Simulations and Observations of Surface Wave Fields under an Extreme Tropical Cyclone. *J. Phys. Oceanogr.* **2009**, *39*, 2097–2116. [[CrossRef](#)]
22. Ardhuin, F.; Rogers, E.; Babanin, A.V.; Filipot, J.F.; Magne, R.; Roland, A.; van der Westhuysen, A.; Queffelec, P.; Lefevre, J.M.; Aouf, L.; et al. Semiempirical Dissipation Source Functions for Ocean Waves. Part I: Definition, Calibration, and Validation. *J. Phys. Oceanogr.* **2010**, *40*, 1917–1941. [[CrossRef](#)]
23. Janssen, P. *The Interaction of Ocean Waves and Wind*; Cambridge University Press: Cambridge, UK, 2004.
24. Komen, G.J.; Hasselmann, S.; Hasselmann, K. On the Existence of a Fully Developed Wind-Sea Spectrum. *J. Phys. Oceanogr.* **1984**, *14*, 1271–1285. [[CrossRef](#)]
25. Rogers, W.E.; Hwang, P.A.; Wang, D.W. Investigation of Wave Growth and Decay in the SWAN Model: Three Regional-Scale Applications. *J. Phys. Oceanogr.* **2003**, *33*, 366–389. [[CrossRef](#)]
26. Hasselmann, K. On the spectral dissipation of ocean waves due to white capping. *Bound. Layer Meteorol.* **1974**, *6*, 107–127. [[CrossRef](#)]
27. Wu, J. Wind-stress coefficients over sea surface from breeze to hurricane. *J. Geophys. Res. Oceans* **1982**, *87*, 9704–9706. [[CrossRef](#)]
28. Huang, Y.; Weisberg, R.H.; Zheng, L.; Zijlema, M. Gulf of Mexico hurricane wave simulations using SWAN: Bulk formula-based drag coefficient sensitivity for Hurricane Ike. *J. Geophys. Res. Oceans* **2013**, *118*, 3916–3938. [[CrossRef](#)]
29. Akbar, M.; Kanjanda, S.; Musinguzi, A. Effect of Bottom Friction, Wind Drag Coefficient, and Meteorological Forcing in Hindcast of Hurricane Rita Storm Surge Using SWAN + ADCIRC Model. *J. Mar. Sci. Eng.* **2017**, *5*, 38. [[CrossRef](#)]
30. Holland, G.J. An Analytic Model of the Wind and Pressure Profiles in Hurricanes. *Mon. Weather Rev.* **1980**, *108*, 1212–1218. [[CrossRef](#)]
31. Moon, I.J.; Ginis, I.; Hara, T.; Tolman, H.L.; Wright, C.W.; Walsh, E.J. Numerical Simulation of Sea Surface Directional Wave Spectra under Hurricane Wind Forcing. *J. Phys. Oceanogr.* **2003**, *33*, 1680–1706. [[CrossRef](#)]
32. Pierce, C.H. The Meteorological History of the New England Hurricane of Sept. 21, 1938. *Mon. Weather Rev.* **1939**, *67*, 237–285. [[CrossRef](#)]
33. Landsea, C.W.; Hagen, A.; Bredemeyer, W.; Carrasco, C.; Glenn, D.A.; Santiago, A.; Strahan-Sakoskie, D.; Dickinson, M. A Reanalysis of the 1931–43 Atlantic Hurricane Database. *J. Clim.* **2014**, *27*, 6093–6118. [[CrossRef](#)]

34. Knaff, J.A.; Zehr, R.M. Reexamination of Tropical Cyclone Wind-Pressure Relationships. *Weather Forecast.* **2007**, *22*, 71–88. [[CrossRef](#)]
35. Vickery, P.J.; Skerlj, P.F.; Twisdale, L.A. Simulation of Hurricane Risk in the U.S. Using Empirical Track Model. *J. Struct. Eng.* **2000**, *126*, 1222–1237. [[CrossRef](#)]
36. Tolman, H.L.; Chalikov, D. Source Terms in a Third-Generation Wind Wave Model. *J. Phys. Oceanogr.* **1996**, *26*, 2497–2518. [[CrossRef](#)]
37. Cavaleri, L. Wave Modeling—Missing the Peaks. *J. Phys. Oceanogr.* **2009**, *39*, 2757–2778. [[CrossRef](#)]
38. The WISE Group. Wave modelling—The state of the art. *Prog. Oceanogr.* **2007**, *75*, 603–674.



© 2018 by the authors. Licensee MDPI, Basel, Switzerland. This article is an open access article distributed under the terms and conditions of the Creative Commons Attribution (CC BY) license (<http://creativecommons.org/licenses/by/4.0/>).